Comparison of Cornea Module and DermaInspect for noninvasive imaging of ocular surface pathologies

Philipp Steven
University Medical Center of Schleswig-Holstein
Department of Ophthalmology
and
University of Luebeck
Institute of Anatomy
Ratzeburger Allee 160
Luebeck 23538 Germany
E-mail: p.steven@uk-sh.de

Maya Müller
University Medical Center of Schleswig-Holstein
Department of Ophthalmology
Ratzeburger Allee 160
Luebeck 23538 Germany

Norbert Koop
University of Luebeck
Institute of Biomedical Optics
Peter-Monnik-Weg 4
Luebeck 23562 Germany

Christian Rose
University Medical Center of Schleswig-Holstein
Department of Dermatology
Ratzeburger Allee 160
Luebeck 23538 Germany

Gereon Hüttmann
University of Luebeck
Institute of Biomedical Optics
Peter-Monnik-Weg 4
Luebeck 23562 Germany

Abstract. Minimally invasive imaging of ocular surface pathologies aims at securing clinical diagnosis without actual tissue probing. For this matter, confocal microscopy (Cornea Module) is in daily use in ophthalmic practice. Multiphoton microscopy is a new optical technique that enables high-resolution imaging and functional analysis of living tissues based on tissue autofluorescence. This study was set up to compare the potential of a multiphoton microscope (DermaInspect) to the Cornea Module. Ocular surface pathologies such as pterygia, papillomae, and nevi were investigated *in vivo* using the Cornea Module and imaged immediately after excision by DermaInspect. Two excitation wavelengths, fluorescence lifetime imaging and second-harmonic generation (SHG), were used to discriminate different tissue structures. Images were compared with the histopathological assessment of the samples. At wavelengths of 730 nm, multiphoton microscopy exclusively revealed cellular structures. Collagen fibrils were specifically demonstrated by second-harmonic generation. Measurements of fluorescent lifetimes enabled the highly specific detection of goblet cells, erythrocytes, and nevus-cell clusters. At the settings used, DermaInspect reaches higher resolutions than the Cornea Module and obtains additional structural information. The parallel detection of multiphoton excited autofluorescence and confocal imaging could expand the possibilities of minimally invasive investigation of the ocular surface toward functional analysis at higher resolutions. [DOI: 10.1117/1.3275475]

Keywords: multiphoton microscopy; confocal microscopy; *in vivo* microscopy; ophthalmology.

Paper 09002RR received Jan. 5, 2009; revised manuscript received Oct. 12, 2009; accepted for publication Oct. 22, 2009; published online Dec. 21, 2009. This paper is a revision of a paper presented at the SPIE conference on Multiphoton Microscopy in the Biomedical Sciences VIII, January 2008, San Jose, California. The paper presented there appears (unrefereed) in SPIE Proceedings Vol. 6860.

1 Introduction

Optical imaging of ocular pathologies is crucial for the clinical diagnosis of ophthalmological diseases. Slit-lamp biomicroscopy is the basic imaging technique used by ophthalmologists for the assessment and diagnosis of ocular pathologies of the anterior and posterior part of the eye, although it is limited in resolution. The introduction of optical coherence tomography (OCT)[1,2] and reflection and fluorescence imaging of the retina opened further possibilities in the diagnosis of retinal disorders by adding information about the retinal microarchitecture and blood supply. However, real microscopic imaging at the posterior segment of the eye is impeded by the limited aperture of the eye. In contrast, imaging the ocular surface is possible with subcellular resolutions. The introduction of confocal microscopy that is based on reflected near-infrared (NIR) light successfully demonstrated high-resolution visualization of the cornea and conjunctiva. Especially, different epithelia as well as fibroblasts, Langerhans cells, and nerve fibers within the transparent cornea[3] and also corneal endothelial cells were distinguished by this technique. Clinical applications include the detection of acanthameba cysts,[4] corneal dystrophies,[5,6] dry eye,[7] contact lens–associated changes,[8,9] and recently stromal alterations following corneal cross-linking.[10] In confocal reflection microscopy, contrast is generated by reflections at interfaces of tissue and cellular structures due to variations of the index of refraction. Nevertheless, it provides only morphological information that enables us to analyze tissue components rather than the functional state of the tissue. In contrast, intrinsic tissue fluorescence, so-called autofluorescence, which is caused by collagen, elastin, NAD(P)H, flavins, etc., provides specific structural and also functional information. Femtosecond radiation in the NIR range from 700 nm to 900 nm can propagate in tissues to a depth of a few hundred micrometers. There, the irradiance in the focal spot may still reach a level

Address all correspondence to: Phillipp Steven, Department of Ophthalmology, University Medical Center of Schleswig-Holstein, Ratzeburger Allee 160, 23538, Luebeck, Germany. Tel: 49-451-5004015; Fax: 49-451-5004034; E-mail: p.steven@uk-sh.de.

1083-3668/2009/14(6)/064040/8/$25.00 © 2009 SPIE

of a few hundred GW/cm^2, at which two photons get simultaneously absorbed.[11,12] The combined energy of the two infrared photons is able to excite tissue autofluorescence only in the focal volume that provides inherent three-dimensional (3-D) sectioning.[13,14] Hence, multiphoton excited fluorescence microscopy is the only method to image tissue autofluorescence in thick living tissues with longitudinal and transverse resolutions better than a micrometer.[15] Besides autofluorescence, multiphoton imaging techniques use second-harmonic generation (SHG) to detect noncentrosymmetric molecules like collagen.[16] Through this, collagen structures in ocular tissues have been visualized with high contrast.[17] Fluorescence lifetime measurement (FLIM) of fluorophores that are present in the tissue combines structural with functional information by analyzing cellular metabolism.[18,19] For clinical *in vivo* applications, the use of autofluorescence seems very appealing, since fluorescence dyes that are approved for *in vivo* use in humans are rare and lack great specificity.

These unique properties suggest the use of multiphoton excited autofluorescence as a multiphoton tomography (MT) in clinical diagnosis. Recently, the Conformité Europeénne (CE)-marked device DermaInspect (DI) was introduced for skin imaging.[20–22] It is currently being tested for tumor diagnosis, visualization of skin aging, and quantification of the uptake of chemical substances or nanoparticles. Nevertheless, clinical diagnosis of the skin by MT has to compete with magnified visual examination and histology of skin biopsies that are routinely taken. In addition, skin areas that might require detailed examination can be quite large, resulting in long investigation times for a microscopic procedure.

A promising field for MT is the ocular surface consisting of cornea, sclera, and conjunctiva. In contrast to the skin, biopsies are not taken as easily from these tissues, due to the lack of excess tissue and impending functional loss, e.g., by postoperative scarring. In this context, it was shown that multiphoton excited autofluorescence and SHG provides clinically useful information about microscopic changes of the cornea that are associated with keratoconus,[23,24] infection,[25] scar formation,[26] and thermal or mechanical damage associated with refractive surgery.[27,28] A recent report showed also complementary information from confocal reflectance and MT in nondiseased cornea.[29] All these studies suggest a potential role of MT in clinical diagnosis of corneal diseases. Nevertheless multiphoton imaging of other ocular surface pathologies besides the cornea have not been done until now.

A microscopic-based preoperative diagnosis is already possible by the Rostock Cornea Module (RCM), a confocal reflectance microscope added on to the retina laser scanner HRT II from Heidelberg Engineering.[3] However, its clinical value is limited because solely morphological information is gained from the tissue that lacks equivalent functional and histopathological data possibly provided by MT.

In order to assess image quality and possible clinical applications of MT, we used the DermaInspect (DI) to image different freshly excised pathologies of the ocular surface and compared the multiphoton images with *in vivo* RCM images of the same individual, taken prior to surgery. The aim of this study was to compare the potential of MT and FLIM with confocal microscopy for imaging ocular structures, especially in nontransparent pathologically changed tissue, and to find new possible diagnostic applications of autofluorescence-based multiphoton microscopy.

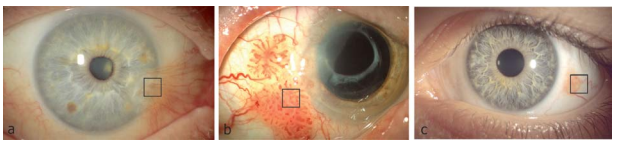

Fig. 1 Ocular surface pathologies: (a) pterygium, (b) conjunctival papilloma, and (c) conjunctival nevus. Squares: areas of interest.

2 Material and Methods

Different ocular surface pathologies (Fig. 1) were investigated *in vivo* by the Rostock Cornea Module in combination with the HRT II (Heidelberg Engineering, Heidelberg, Germany). After surgical excision, the pathologies were stored in tissue culture media and immediately investigated by the multiphoton tomograph DermaInspect (JenLab GmbH, Neuengönna, Germany) without further fixation. The DermaInspect consisted of a solid-state, mode-locked 80-MHz titanium:sapphire laser (MaiTai, Spectra Physics, Darmstadt, Germany) with a tuning range of 710 to 920 nm and a mean laser output of >900 mW at 800 nm that delivered a pulse width of approximately 150 fs to the sample. Tissue autofluorescence was imaged by exciting the samples at 730 and 835 nm, respectively. The DermaInspect contained a computer-controlled beam attenuator, a shutter, and a two-axis galvoscanner. A 40× objective with NA 1.3 and 140-μm working distance (Plan-Neofluar 40×, 1.3 Oil, Zeiss, Göttingen, Germany), which was focused by a piezodriven holder, was used in this study. Larger scale motions of the sample in the x and y directions were performed by computer-controlled steppermotors (Owis GmbH, Staufen, Germany). The autofluorescence was detected by a standard photomultiplier module (H7732, Hamamatsu, Herrsching, Germany) after passing through a beamsplitter (Chroma 640 DCSPXR, AHF Analysentechnik AG, Tübingen) and a short-pass filter (BG39, Schott, Mainz, Germany), resulting in a detection bandwidth from 380 to 530 nm (FWHM), which could not detect the second-harmonic generation (SHG) signal for an excitation shorter than 760 nm. To detect SHG, the excitation was tuned to 826 nm in order to maximize SHG signal strength[30] and transmission of the optics, which were designed for the visible range, and the same photomultiplier with a 413-nm bandpass filter (Amko, Tornesch, Germany) was used for suppression of autofluorescence.

Fluorescence lifetime imaging (FLIM) was performed by time-correlated single-photon counting.[31] Start signals were generated from a fast photomultiplier module (PMH-100-0, Becker & Hickl, Berlin, Germany) with a transient time spread of approximately 180 ps that detected the fluorescence photons emitted by the tissue. The stop signal was provided by a fast photodiode that measured the excitation pulses. The timing between both signals was measured by a PC-based single-photon counting board (SPC 830, Becker & Hickl, Berlin, Germany). The board was synchronized with the scanning of the excitation beam, and 256×256 spatially resolved autofluorescence decay curves were measured in the image field. Curve fitting with a single exponential decay curve including

Table 1 Comparison of the technical specifications of the HRT with Cornea Module and the DermaInspect.

	Rostock Cornea Module+HRTII (RCM)	DermaInspect (DI)
Technical background and working principle	Confocal microscope	Multiphoton microscope
	Diode laser 670 nm	Femtosecond laser 710–900 nm
	Reflection contrast	Autofluorescence, SHG, FLIM
Specifications	*In vivo* human patients	*In vivo* human skin, *ex vivo* samples
	NA: 0.9 water immersion	NA: 1.3 oil immersion
	Focus size: 0.91 μm×4.1 μm, 1–30 frames/s	Focus size: 0.69 μm×1.6 μm, 0.02–1.0 frames/s
	Field of view 300–400 μm	Field of view 20–230 μm
	Single images, stacks, video	Single images, stacks, SHG, FLIM

a deconvolution with the time response of the system (SPCImage 2.6, Becker & Hickl, Berlin, Germany) was used to calculate a mean fluorescence lifetime for each pixel and was displayed in color-coded images.

After imaging, the specimens were sent for definite histopathological assessment. The tissue was fixed, sliced in 5-μm sections, and stained with haematoxyline eosin (H.E.). The study was conducted according to the Declaration of Helsinki and approved by the Ethics Committee of the University of Luebeck (08-083), and informed consent was obtained prior the procedure from each patient.

3 Results and Discussion

Due to the working principle and the intended use, RCM and DI have different technical characteristics (Table 1). To carry out confocal imaging with reflectance contrast, a relatively inexpensive diode laser is sufficient, whereas the DermaInspect uses a tunable femtosecond laser to generate autofluorescence, SHG, and fluorescence lifetime images. Both systems work with different commercially available microscope objectives. The RCM uses a 63×, NA 0.95 water immersion objective that gives a diffraction-limited focal spot of 0.9 μm

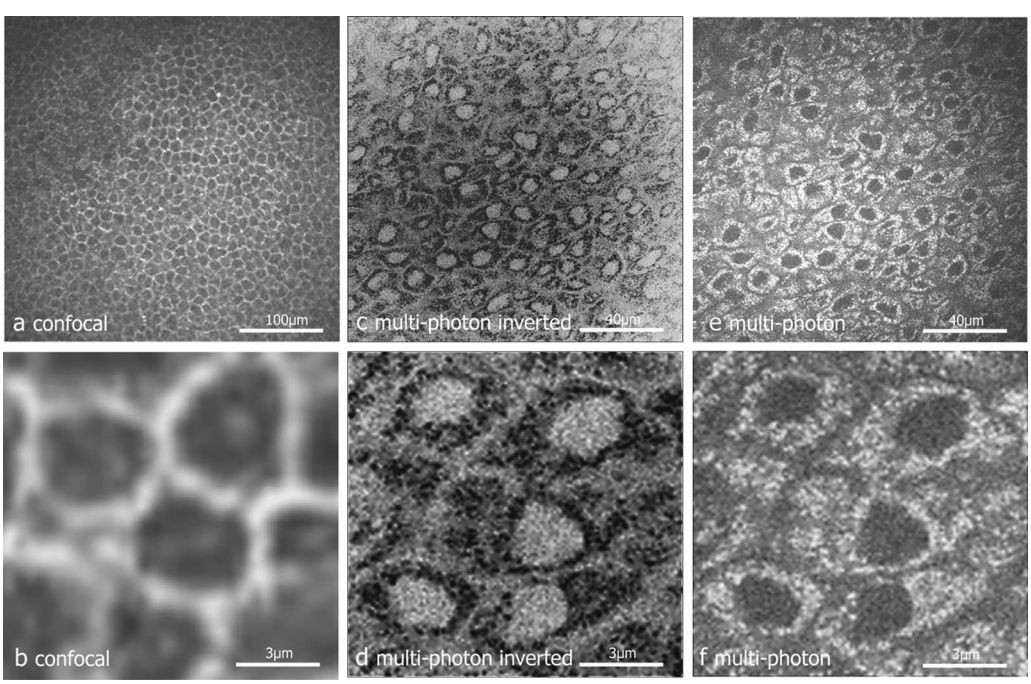

Fig. 2 Epithelial cells of the cornea. (a) and (b): Imaged with confocal microscopy (HRTII+Rostock Cornea Module). (c) and (f) Imaged with multiphoton microscopy (DermaInspect). Images (b), (d), and (f) show a digitally magnified, view from (a), (c), and (e). (c) and (d): Digitally inverted images (e) and (f).

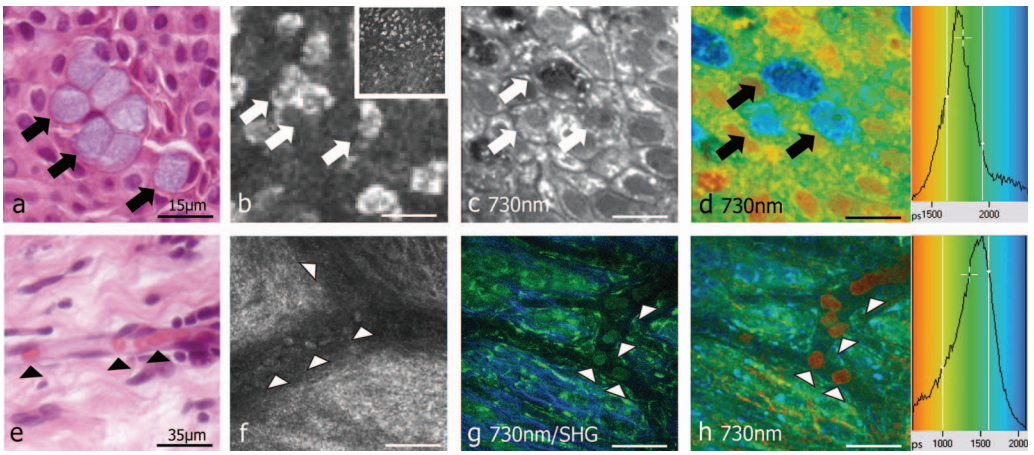

Fig. 3 Pterygium. (a) to (d): Goblet cells within the epithelium (arrows). (a) Histology, H.E. stain; (b) confocal image; (c) multiphoton intensity image; and (d) fluorescence lifetime imaging (lifetime histogram in ps). (e) to (h) Blood vessels filled with erythrocytes (arrows). (e) Histology, H.E. stain; (f) confocal image; (g) composite image of multiphoton microscopy (false color labeling, 730 nm: green, SHG: blue); and (h) fluorescence lifetime imaging (lifetime histogram in ps).

(diameter of the Airy disk) and a length of the focal volume of 4.1 μm (Ref. 3). The field of view can be varied between 300 μm and 400 μm. The DI works at a higher resolution due to the 40×, NA 1.3 oil immersion objective, which can provide a limited focus volume of 0.68 μm × 1.6 μm at 730-nm diffraction. Corresponding to the increased resolution, the field of view is smaller (20 μm to 230 μm). The RCM achieves video rate imaging with up to 30 frames per second. Due to the lower autofluorescence signals, the maximal imaging speed of the DI is limited to less than 1 frame per second at quite restricted image quality. For high-quality images, as shown in Figs. 2–5, exposure times of 25 s were necessary. For multiphoton imaging, the image acquisition time is limited by the excitation threshold for tissue damage, which is only a factor of two from the excitation intensity used. A possible solution to this limitation would be to use multiple scanning beams. However, due to cross talk, the image quality rapidly degrades with depth in scattering tissues. Only for the transparent cornea can no reduction of image quality be expected.

Both devices acquire single images and image stacks with variable z spacing. In addition, the RCM has the option to generate videos of dynamic tissue changes.

The practical resolution of both systems, RCM and DI, was assessed with images from corneal epithelial cells. Both devices provided subcellular resolution. The RCM was able to resolve the individual cells with bright cell borders and nuclei [Figs. 2(a) and 2(b)]. Structures in the cytoplasm were barely resolved. The DI provided a significantly higher resolution, which allowed us to identify even single-cell organelles. Under multiphoton excitation, the cytoplasm appeared as a granular structure [Figs. 2(e) and 2(f)]. Nuclei and actual cell borders remained dark. Contrast inverted (negative image), the multiphoton images showed some similarities to the con-

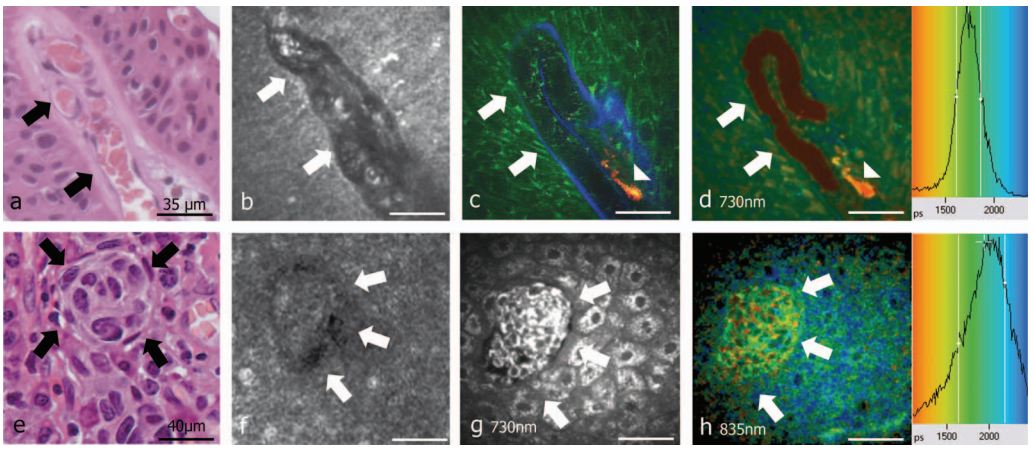

Fig. 4 (a) to (d): Conjunctival papilloma; core blood vessel (arrows) and surrounding papilloma cells (histology, H.E. stain); (b) confocal image; (c) composite image of multiphoton microscopy (false color labeling; 730 nm: green, 835 nm: red, SHG: blue); (d) fluorescence lifetime image (lifetime histogram in ps). (e) to (h): Conjunctival nevus; pigmented nevus-cells form clusters within the epithelium (arrows); (e) histology, H.E. stain; (f) confocal image; (g) multiphoton intensity image; and (h) fluorescence lifetime image (lifetime histogram in ps).

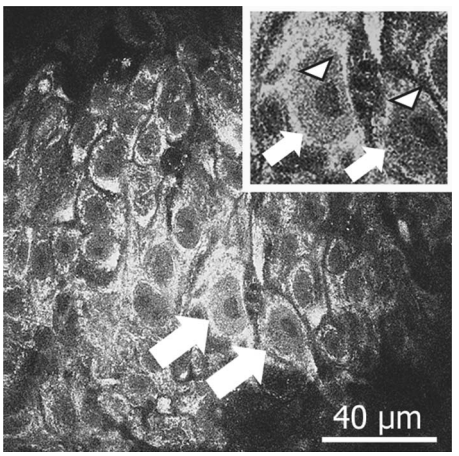

Fig. 5 Conjunctival papilloma cells, multiphoton intensity image; arrows indicate nuclei Inset; arrows indicate nuclei; arrowheads indicate nucleoli.

focal images [Figs. 2(c) and 2(d)]. In epithelial cells, at 730-nm excitation, a prominent source of the autofluorescence in the cytoplasm is NAD(P)H, which is mainly localized in the mitochondria. Shape, size, density, and distribution of mitochondria within the cytoplasm together with shape and size of nucleus and cellular body can be used to discriminate different cell types. Fibroblasts, e.g., demonstrate an elongated dark nucleus with only a small rim of bright fluorescing mitochondria in comparison to epithelial cells that have numerous evenly distributed mitochondria within a broad cytoplasmic rim encircling a roundish nucleus.

Resolution and contrast of the RCM images are significantly poorer than the multiphoton images of the DI. This is explained by the differences in focal spot size and the process of image formation[32] and the lower NA of the objective used. In contrast to confocal imaging, multiphoton imaging has no trade-off between resolution and image brightness. A smaller focus even increases image brightness. In addition, autofluorescence of the mitochondria provides a high-contrast signal on a low background. By using an oil immersion objective, we expect essentially aberration-free imaging in the superficial layers of the tissue, although at deeper layers, the refractive index mismatches between sample and oil reduce the image quality due to spherical aberrations. Fluorescence imaging has further advantages over confocal reflectance imaging. It is incoherent and therefore does not suffer from speckle noise. The high coherence of the laser in confocal reflection imaging leads to speckle noise from interference of scattered light. A higher resolution and better contrast of MT was seen essentially in all images of the investigated tissue structure.

The first noncorneal pathology investigated with confocal and multiphoton imaging was a pterygium, which is a strand of conjunctiva growing onto the cornea [Fig. 1(a) Figs. 3(a)–3(h)]. This tissue contains different cell types, vessels, and connective tissue that were identified by comparative histology [Figs 3(a) and 3(e)]. Mucous-producing goblet cells were easily discriminated in histology from epithelial cells by their special morphology and staining characteristics [Fig. 3(a)]. With the RCM, goblet cells are identified as cells with a hyperreflective cell body compared to surrounding epithelial cells [Fig. 3(b)]. In the autofluorescence images of the DI, goblet cells were clearly seen, as the mucous-filled vacuoles demonstrated very low autofluorescence, even lower than adjacent nuclei [Fig. 3(c)]. In addition, multiphoton-excited FLIM was able to increase the contrast [Fig. 3(d)] and differentiate the cell body of the goblet cells from nuclei, because the mucous within the goblet cells was characterized by a longer (blue) and the nuclei by a shorter fluorescence lifetime (red), compared to the cytoplasm (green) and the mitochondria (yellow). The autofluorescence properties of goblet cells were not yet studied, and the chromophores involved are not known.

Also extracellular structures were visualized by the DI with high resolution. Elastin fibers were seen due to their autofluorescence at 730-nm excitation [green; Fig. 3(g)], whereas straight collagen fibers were seen by SHG imaging [blue; Fig. 3(g)]. RCM images of the connective tissue show straight lines that are probably collagen fibers. These cannot be distinguished from other connective tissue components. Embedded vessels are visible as dark structures in which individual blood cells are located [Fig. 3(f)]. The DI is also able to visualize blood vessels. The femtosecond irradiation excites the autofluorescence of erythrocytes, which is characterized by a very short lifetime (red) [Fig. 3(h)]. The fluorescence is possibly caused by hemoglobin, which is a high multiphoton absorption cross section[33,34] but a low fluorescence quantum yield. From intravital animal experiments, we know that in the *in vivo* situation, imaging with the DI is not fast enough to follow the movement of an individual blood cell, but vessels are still detectable by morphological features and due to characteristic movement artifacts. Vessels were also visualized by SHG of perivascular collagen, as shown in images of an ocular papilloma with a core vessel [Fig. 1(b); Figs. 4(a)–4(d)]. The false color overlay of the autofluorescence [Fig. 4(c); 730 nm: green; 835 nm: red; and SHG: blue] gives the exact co-localization between the cellular and extracellular structures and a clearer image compared to the confocal image [Fig. 4(b)]. At 730-nm and 835-nm excitation, strong fluorescing lysosomes of a perivascular macrophage were visible (here shown yellow/red in the overlay of green and red).

Cellular autofluorescence is caused by a variety of different chromophores,[35] which have different multiphoton excitation efficacies at different wavelengths.[36,37] By changing the excitation wavelength, the contribution of the chromophores to the autofluorescence also changes. NADH, which is responsible for the strong autofluorescence of the mitochondria in epithelial cells, is more efficiently excited at shorter wavelengths below 780 nm. Our work in different tissue shows that excited above 830 nm the NADH fluorescence is very weak, whereas lysosomes, dendritic cells, and macrophages fluoresce quite strongly (work not published). We attribute the fluorescence to flavoproteins,[38] cellular lipids, and aging proteins such as ceroids and lipofuscin.[39,40] Therefore, we conclude that the structure visible at both 730-nm and 835-nm excitation is a macrophage. Dendritic cells, which have similar features, are generally not found in this location. The FLIM image of the same tissue demonstrated short lifetimes of these lysosomes (red) within the macrophage [Fig. 4(d)].

Autofluorescence of melanin was recorded in an ocular nevus [Fig. 1(c) Figs. 4(e)–4(h)]. A bright fluorescence pattern in epithelial cells was observed in a pigmented lesion [Fig. 4(g)]. A distinction from mitochondria or lysosomal fluorescence was achieved by FLIM at 835 nm [Fig. 4(h)]. The fluorescence lifetime of melanosomes (red/yellow) is shorter than the time resolution of our system, which is a few hundred picoseconds with our detector. The RCM demonstrated the same intraepithelial nevus-cell cluster, but the reflection image showed a much lesser contrast and resolution than the DI images. Here, detection was achieved only by shape and the hyporeflective rim around the cluster.

Intercellular structures of cells were visualized by the DI with resolutions that allowed the discrimination between nuclei and prominent nucleoli and the estimation of the cytoplasmic/nuclear ratio (Fig. 5).

The value of fluorescence lifetime imaging (FLIM) for feature identification and clinical diagnosis is currently under evaluation. In principle, FLIM provides additional independent information besides the spectral characteristics of excitation and emission. But it also adds complexity and increases the measurement time if good image quality is desired. Our study suggests that FLIM can indeed provide additional information. Collagen, melanosomes, and erythrocytes are characterized by very short lifetime below 200 ps, which gives a very strong contrast against the 1.5- to 2-ns autofluorescence lifetime of other components. SHG imaging of collagen does not require additional FLIM because it is easily discriminated with a bandpass filter at twice the excitation wavelength from autofluorescence. Melanosomes and erythrocytes do not have a sharp spectral signature.[33,41] In addition, fluorescence intensity of the erythrocytes is quite low, which makes a spectral discrimination difficult. In contrast to this, melanosomes appear as point-like structures that are difficult to discriminate from lysosomes and mitochondria. Here, a good FLIM contrast is important for an identification of these structures. FLIM also allowed discriminating low fluorescing parts of goblet cells from nuclei, as demonstrated in Fig. 3(d).

4 Conclusions

This study compared imaging of ocular surface pathologies by means of confocal reflectance and multiphoton excited autofluorescence microscopy under identical conditions as far as possible using a clinical approved confocal microscope and a multiphoton microscope approved solely for skin imaging *in vivo*.

Both imaging modalities were able to visualize cellular and extracellular structures of ocular tissue pathologies. In the skin, confocal reflectance and multiphoton imaging reach comparable depths. Both can image down into the upper dermis.[20,42] A similar imaging depth with small advantages for the DI was also observed in this study at scattering tissues, but we did not quantify it.

Due to the higher NA of the objective used and the specific nature of fluorescence imaging, DermaInspect images contain more tissue-specific information. The DI was able to resolve subcellular structures like mitochondria or lysosomes that were barely seen by the RCM. Also size and shape of the nuclei were imaged with considerably higher precision. Even nucleoli were visualized. High contrast and the lack of speckle noise contributed to the considerably higher morphological information content of subcellular structures. Hereby, different cell types such as goblet cells and epithelial cells can be distinguished with high specificity. In principle, comparable resolution and image quality are also possible in confocal reflectance microcopy by using a high NA immersion objective and by averaging multiple images for speckle reduction. However, the four parameters (fluorescence intensity, spectrum, excitation, and FLIM) of the autofluorescence, which are measured by the DI, provide additional information for characterization and identification of tissue structures that is not available in reflectance microcopy. This enables a unique characterization of cellular and tissue components such as mitochondria, hemoglobin, collagen, or melanin. We demonstrated spectral and fluorescence lifetime–based identification of epithelial cells, goblet cells, erythrocytes, macrophages, collagen, elastin, vascular structures, and pigmented lesions.

The possibility to measure unique fluorescence signatures for these structures paves the way for an automatic identification of tissue structures, which is difficult when it has to be based solely on morphological features. In this context, we have demonstrated previously that the dependence of the fluorescence lifetime on the excitation wavelength can discriminate different brain tissues and different tumor cells lines.[43,44] NAD(P)H–based FLIM has the potential to differentiate cell type or even stages of cell development, since it can monitor *in vivo* NAD(P)H–dependent cellular metabolism.[45] Possible applications in diagnosing ocular surface pathologies include detection of pathogens in inflammatory diseases, characterization of immune cells (lymphocytes, macrophages, etc.) during ocular surface inflammation, detection of epithelial neoplasias of conjunctiva and cornea by measuring a shifted nucleoplasmic index, and detection of tumor cells that demonstrate an enhanced cellular metabolism. The main disadvantage of multiphoton versus confocal microscopy—besides the currently expensive equipment—is a slow imaging speed caused by a principally limited fluorescence rate from one focal spot. Multifocal spot scanning[46,47] adds complexity and suffers strongly from degraded contrast in deeper scattering tissue. An alternative solution to this problem is to combine multiphoton with confocal microscopy. This approach would allow scanning larger regions by confocal microscopy, identifying certain small regions of interest and restricting the spectrally resolved multiphoton imaging to these small areas. Based on the results presented, our next step will be to integrate multiphoton imaging into a clinical instrument for *in vivo* imaging.

Acknowledgments

We thank Heidelberg Engineering GmbH for providing the HRT II with Cornea Module for this study. This study was supported by University of Luebeck Medical Technology Research Grant Nos. A6 2006-2007 and SPP TP3 2009-2010.

References

1. D. Huang, E. A. Swanson, C. P. Lin, J. S. Schuman, W. G. Stinson, W. Chang, M. R. Hee, T. Flotte, K. Gregory, C. A. Puliafito et al., "Optical coherence tomography," *Science* **254**(5035), 1178–1181 (1991).
2. M. E. van Velthoven, D. J. Faber, F. D. Verbraak, T. G. van Leeuwen, and M. D. de Smet, "Recent developments in optical coherence to-

mography for imaging the retina," *Prog. Retin Eye Res.* **26**(1), 57–77 (2007).
3. R. Guthoff, J. Stave, and C. Baudouin, *Atlas of Confocal Laser Scanning "In Vivo" Microscopy in Ophthalmology*, Springer, Berlin (2006).
4. Y. Matsumoto, M. Dogru, E. A. Sato, Y. Katono, Y. Uchino, S. Shimmura, and K. Tsubota, "The application of *in vivo* confocal scanning laser microscopy in the management of *Acanthamoeba* keratitis," *Mol. Vis* **13**, 1319–1326 (2007).
5. A. Kobayashi and K. Sugiyama, "*In vivo* laser confocal microscopy findings for Bowman's layer dystrophies (Thiel-Behnke and Reis-Bucklers corneal dystrophies)," *Ophthalmology* **114**(1), 69–75 (2007).
6. D. V. Patel, C. N. Grupcheva, and C. N. McGhee, "Imaging the microstructural abnormalities of Meesmann corneal dystrophy by *in vivo* confocal microscopy," *Cornea* **24**(6), 669–673 (2005).
7. B. Erdelyi, R. Kraak, A. Zhivov, R. Guthoff, and J. Nemeth, "*In vivo* confocal laser scanning microscopy of the cornea in dry eye," *Graefes Arch. Clin. Exp. Ophthalmol.* **245**(1), 39–44 (2007).
8. N. Efron, H. A. Mutalib, I. Perez-Gomez, and H. H. Koh, "Confocal microscopic observations of the human cornea following overnight contact lens wear," *Clin. Exp. Optom.* **85**(3), 149–155 (2002).
9. N. Efron, I. Perez-Gomez, and P. B. Morgan, "Confocal microscopic observations of stromal keratocytes during extended contact lens wear," *Clin. Exp. Optom.* **85**(3), 156–160 (2002).
10. R. Mencucci, C. Mazzotta, F. Rossi, C. Ponchietti, R. Pini, S. Baiocchi, A. Caporossi, and U. Menchini, "Riboflavin and ultraviolet A collagen crosslinking: *in vivo* thermographic analysis of the corneal surface," *J. Cataract Refractive Surg.* **33**(6), 1005–1008 (2007).
11. W. Denk, J. H. Strickler, and W. W. Webb, "Two-photon laser scanning fluorescence microscopy," *Science* **248**(4951), 73–76 (1990).
12. F. Helmchen and W. Denk, "Deep tissue two-photon microscopy," *Nat. Methods* **2**(12), 932–940 (2005).
13. D. W. Piston, "Imaging living cells and tissues by two-photon excitation microscopy," *Trends Cell Biol.* **9**(2), 66–69 (1999).
14. M. Rubart, "Two-photon microscopy of cells and tissue," *Circ. Res.* **95**(12), 1154–1166 (2004).
15. C. Y. Dong, K. Koenig, and P. So, "Characterizing point spread functions of two-photon fluorescence microscopy in turbid medium," *J. Biomed. Opt.* **8**(3), 450–459 (2003).
16. P. J. Campagnola, A. C. Millard, M. Terasaki, P. E. Hoppe, C. J. Malone, and W. A. Mohler, "Three-dimensional high-resolution second-harmonic generation imaging of endogenous structural proteins in biological tissues," *Biophys. J.* **82**(1 Pt 1), 493–508 (2002).
17. S. W. Teng, H. Y. Tan, J. L. Peng, H. H. Lin, K. H. Kim, W. Lo, Y. Sun, W. C. Lin, S. J. Lin, S. H. Jee, P. T. So, and C. Y. Dong, "Multiphoton autofluorescence and second-harmonic generation imaging of the *ex vivo* porcine eye," *Invest. Ophthalmol. Visual Sci.* **47**(3), 1216–1224 (2006).
18. V. Ulrich, P. Fischer, I. Riemann, and K. Konig, "Compact multiphoton/single photon laser scanning microscope for spectral imaging and fluorescence lifetime imaging," *Scanning* **26**(5), 217–225 (2004).
19. D. K. Bird, L. Yan, K. M. Vrotsos, K. W. Eliceiri, E. M. Vaughan, P. J. Keely, J. G. White, and N. Ramanujam, "Metabolic mapping of MCF10A human breast cells via multiphoton fluorescence lifetime imaging of the coenzyme NADH," *Cancer Res.* **65**(19), 8766–8773 (2005).
20. K. Konig and I. Riemann, "High-resolution multiphoton tomography of human skin with subcellular spatial resolution and picosecond time resolution," *J. Biomed. Opt.* **8**(3), 432–439 (2003).
21. F. Stracke, B. Weiss, C. M. Lehr, K. Konig, U. F. Schaefer, and M. Schneider, "Multiphoton microscopy for the investigation of dermal penetration of nanoparticle-borne drugs," *J. Invest. Dermatol.* **126**(10), 2224–2233 (2006).
22. M. J. Koehler, K. Konig, P. Elsner, R. Buckle, and M. Kaatz, "*In vivo* assessment of human skin aging by multiphoton laser scanning tomography," *Opt. Lett.* **31**(19), 2879–2881 (2006).
23. H. Y. Tan, Y. Sun, W. Lo, S. J. Lin, C. H. Hsiao, Y. F. Chen, S. C. Huang, W. C. Lin, S. H. Jee, H. S. Yu, and C. Y. Dong, "Multiphoton fluorescence and second harmonic generation imaging of the structural alterations in keratoconus *ex vivo*," *Invest. Ophthalmol. Visual Sci.* **47**(12), 5251–5259 (2006).
24. N. Morishige, A. J. Wahlert, M. C. Kenney, D. J. Brown, K. Kawamoto, T. Chikama, T. Nishida, and J. V. Jester, "Second-harmonic imaging microscopy of normal human and keratoconus cornea," *Invest. Ophthalmol. Visual Sci.* **48**(3), 1087–1094 (2007).
25. H. Y. Tan, Y. Sun, W. Lo, S. W. Teng, R. J. Wu, S. H. Jee, W. C. Lin, C. H. Hsiao, H. C. Lin, Y. F. Chen, D. H. Ma, S. C. Huang, S. J. Lin, and C. Y. Dong, "Multiphoton fluorescence and second harmonic generation microscopy for imaging infectious keratitis," *J. Biomed. Opt.* **12**(2), 024013 (2007).
26. S. W. Teng, H. Y. Tan, Y. Sun, S. J. Lin, W. Lo, C. M. Hsueh, C. H. Hsiao, W. C. Lin, S. C. Huang, and C. Y. Dong, "Multiphoton fluorescence and second-harmonic-generation microscopy for imaging structural alterations in corneal scar tissue in penetrating full-thickness wound," *Arch. Ophthalmol. (Chicago)* **125**(7), 977–978 (2007).
27. T. J. Wang, W. Lo, C. M. Hsueh, M. S. Hsieh, C. Y. Dong, and F. R. Hu, "*Ex vivo* multiphoton analysis of rabbit corneal wound healing following conductive keratoplasty," *J. Biomed. Opt.* **13**(3), 034019 (2008).
28. M. Farid, N. Morishige, L. Lam, A. Wahlert, R. F. Steinert, and J. V. Jester, "Detection of corneal fibrosis by imaging second harmonic-generated signals in rabbit corneas treated with mitomycin C after excimer laser surface ablation," *Invest. Ophthalmol. Visual Sci.* **49**(10), 4377–4383 (2008).
29. W. L. Chen, Y. Sun, W. Lo, H. Y. Tan, and C. Y. Dong, "Combination of multiphoton and reflective confocal imaging of cornea," *Microsc. Res. Tech.* **71**(2), 83–85 (2008).
30. N. Morishige, W. M. Petroll, T. Nishida, M. C. Kenney, and J. V. Jester, "Noninvasive corneal stromal collagen imaging using two-photon-generated second-harmonic signals," *J. Cataract Refractive Surg.* **32**(11), 1784–1791 (2006).
31. W. Becker, *Advanced Time-Correlated Single Photon Counting Techniques*, Springer, Berlin, Heidelberg, and New York (2005).
32. G. Cox and C. J. Sheppard, "Practical limits of resolution in confocal and non-linear microscopy," *Microsc. Res. Tech.* **63**, 18–22 (2004).
33. J. R. Zhang, Y. W. Xu, Y. M. Deng, C. K. Wu, S. P. Jiang, and S. H. Lian, "Laser-induced multiphoton fluorescence of hemoglobin," *J. Photochem. Photobiol., B* **1**(3), 329–335 (1988).
34. G. O. Clay, C. B. Schaffer, and D. Kleinfeld, "Large two-photon absorptivity of hemoglobin in the infrared range of 780–880 nm," *J. Chem. Phys.* **126**(2), 025102 (2007).
35. G. A. Wagnieres, W. M. Star, and B. C. Wilson, "*In vivo* fluorescence spectroscopy and imaging for oncological applications," *Photochem. Photobiol.* **68**, 603–632 (1998).
36. W. R. Zipfel, R. M. Williams, R. Christie, A. Y. Nikitin, B. T. Hyman, and W. W. Webb, "Live tissue intrinsic emission microscopy using multiphoton-excited native fluorescence and second harmonic generation," *Proc. Natl. Acad. Sci. U.S.A.* **100**(12), 7075–7080 (2003).
37. S. Huang, A. A. Heikal, and W. W. Webb, "Two-photon fluorescence spectroscopy and microscopy of NAD(P)H and flavoprotein," *Biophys. J.* **82**(5), 2811–2825 (2002).
38. R. C. Benson, R. A. Meyer, M. E. Zaruba, and G. M. McKhann, "Cellular autofluorescence—is it due to flavins?," *J. Histochem. Cytochem.* **27**(1), 44–48 (1979).
39. J. D. Edelson, D. K. MacFadden, M. Klein, and A. S. Rebuck, "Autofluorescence of alveolar macrophages: problems and potential solutions," *Med. Hypotheses* **17**(4), 403–407 (1985).
40. J. M. Njoroge, L. B. Mitchell, M. Centola, D. Kastner, M. Raffeld, and J. L. Miller, "Characterization of viable autofluorescent macrophages among cultured peripheral blood mononuclear cells," *Cytometry* **44**(1), 38–44 (2001).
41. K. Teuchner, W. Freyer, D. Leupold, A. Volkmer, D. J. Birch, P. Altmeyer, M. Stucker, and K. Hoffmann, "Femtosecond two-photon excited fluorescence of melanin," *Photochem. Photobiol.* **70**(2), 146–151 (1999).
42. A. L. Branzan, M. Landthaler, and R. M. Szeimies, "*In vivo* confocal scanning laser microscopy in dermatology," *Lasers Med. Sci.* **22**(2), 73–82 (2003).
43. S. R. Kantelhardt, J. Leppert, J. Krajewski, N. Petkus, E. Reusche, V. M. Tronnier, G. Huttmann, and A. Giese, "Imaging of brain and brain tumor specimens by time-resolved multiphoton excitation microscopy *ex vivo*," *J. Neuro-Oncol.* **9**(2), 103–112 (2007).
44. J. Leppert, J. Krajewski, S. R. Kantelhardt, S. Schlaffer, N. Petkus, E. Reusche, G. Huttmann, and A. Giese, "Multiphoton excitation of autofluorescence for microscopy of glioma tissue," *Neurosurgery* **58**(4), 759–767 (2006).

45. D. W. Piston, B. R. Masters, and W. W. Webb, "Three-dimensionally resolved NAD(P)H cellular metabolic redox imaging of the in situ cornea with two-photon excitation laser scanning microscopy," *J. Microsc.* **178**(Pt 1), 20–27 (1995).
46. T. Nielsen, M. Fricke, D. Hellweg, and P. Andresen, "High efficiency beam splitter for multifocal multiphoton microscopy," *J. Microsc.* **201**(Pt 3), 368–376 (2001).
47. K. H. Kim, C. Buehler, K. Bahlmann, T. Ragan, W.-C. A. Lee, E. Nedivi, E. L. Heffer, S. Fantini, and P. T. C. So, "Multifocal multiphoton microscopy based on multianode photomultiplier tubes," *Opt. Express* **15**(18), 11658–11678 (2007).